46th Annual Review of Progress in Quantitative Nondestructive Evaluation
QNDE2019
July 14-18, 2019, Portland, OR, USA

QNDE2019-6967

CHARACTERIZING POLYMER O-RINGS NONDESTRUCTIVELY USING RESONANT ULTRASOUND SPECTROSCOPY

Richard Livings[1], William Bachman, Eric Biedermann
Vibrant Corp.
Albuquerque, NM

ABSTRACT

Polymer O-rings are an essential part of many designs, including mission and safety critical systems. Currently, there are no accurate destructive tests for measuring the polymer properties of O-rings (e.g. durometer), let alone nondestructive methods. As such, it is difficult to identify substandard, nonconforming, improperly processed or counterfeit O-rings. This work combines resonant ultrasound spectroscopy (RUS) with machine learning and predictive analytics to sort O-rings based on material and durometer (multinomial classification) and to accurately estimate the mass and durometer with an ultrasonic examination that takes less than 10 seconds. Results from a population including eight materials and six durometers are presented and discussed.

Keywords: Resonance, Resonant Ultrasound Spectroscopy, RUS, Polymer, Machine Learning

1 INTRODUCTION

Detecting substandard, nonconforming, improperly processed, or counterfeit parts has become an increasingly important topic for private companies and government agencies alike. Polymer O-rings are essential to many mission and safety critical systems. Detection of unacceptable O-rings is hampered by the lack of effective nondestructive evaluation (NDE) methods for this application. A fast, accurate, and reliable NDE method for O-rings is needed to guarantee safety and mission success.

Substandard, nonconforming, improperly processed, or counterfeit parts, colloquially referred to as Suspected Unapproved Parts (SUP), are present in nearly every industry, but the likely loss of life due to SUP is probably highest in the aerospace industry. Groups like the AIA (Aerospace Industries Association) have been trying to draw attention to the dangers of SUP for several years [1].

An internal 1995 FAA audit estimated that more than 500,000 unacceptable parts are installed on aircraft each year [2]. An additional study by the FAA of its Accident and Incident Data System (AIDS) database specified 147 accidents/incidents were attributable to SUP between 1973 and 1996 [3]. Later, a review of the NTSB accident database found nearly two dozen accidents attributable to SUP between 2010 and 2017 [4]. In fact, Baker estimated that SUP accidents and incidents continue to occur at a rate of ~2.3 per year [5].

In 1995, the FAA implemented SUP detection plan [6], but an OIG review in 2017 concluded that the detection activities were practically ineffectual and recommended significant enhancements [7].

In addition to the accidents that occurred due to SUP, there have been multiple cases were SUP was detected before installation. In fact, there have been multiple cases of contractors and subcontractors selling counterfeit polymeric O-rings to US government agencies [8], [9].

The reason polymeric O-rings are so easy to counterfeit is their similarity in visual appearance. Several of the largest manufacturers of polymer O-rings recognize the extensive problem of counterfeit O-rings and the difficulty with identification and testing. These manufacturers have proposed various solutions from QR codes [10] to imbedded RFID tags [11].

Currently, there are no accurate and reliable methods to measure the durometer of an O-ring or to nondestructively characterize its material [12], [13], [14]. The standard durometer measurement method is a semi-destructive Shore hardness A test, which is not applicable to O-rings. The applicable method (Shore M) is a semi-destructive micro-harness test and is not accurate or reliable due to the deformation of the O-ring during testing. Existing material characterization methods, like Fourier Transform Infrared Spectroscopy (FTIR), are slow, labor-intensive, open to interpretation errors, and can be destructive.

An alternative approach to material characterization and durometer measurement in O-rings is needed. By characterizing the filtering effects of O-rings on a resonance spectrum, extracting signal features, and analyzing with machine learning,

[1] Contact author: rlivings@vibrantndt.com

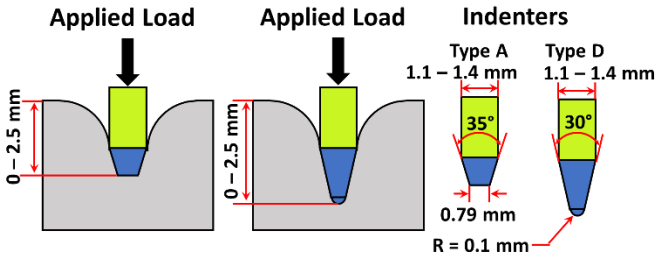

FIGURE 1: DIAGRAM OF DUROMETER TESTING.

material and durometer differences between O-rings can be distinguished.

This paper presents a novel nondestructive method for determining the material, durometer, and mass of polymer O-rings using RUS and a Random Forest machine learning algorithm. Using this approach, O-rings were accurately sorted into eleven material-durometer classifications, their durometer was accurately estimated to within the standard tolerance, and their mass was accurately estimated to within the measurement error.

2 BACKGROUND

As stated by one of the leading manufacturers of O-rings, O-rings are nearly identical and very difficult to distinguish from each other [11]. Industry standard O-ring characterization includes measurements for hardness, toughness, tensile strength, elongation, compression force, and many others. Unfortunately, the vast majority of these are destructive and are performed on a limited sampling of O-rings. This leads to a dearth of options for sorting, characterizing, or verifying O-ring conformity nondestructively.

2.1 Current NDE Methods

The two most common approaches to classifying O-rings are the Shore hardness test and Fourier Transform Infrared Spectroscopy (FTIR) [12]. Both of these methods are debatably nondestructive, rely on limited sampling, have some significant limitations, and are much less likely to provide accurate results than 100% testing using the resonance method presented here.

Shore hardness testing is an indentation method with multiple scales depending on the indentation head and load. Shore A, D, and M are the most common where M is a much smaller indentation head. FIGURE 1 demonstrates the differences between type A and type D while FIGURE 2 provides a qualitative comparison of the various scales. Note that

TABLE 1: UNCERTAINTY OF SHORE HARDNESS TESTERS (A & D). RECREATED FROM [18].

Durometer	u_c	U
30	1.4639	2.94
50	1.4731	4.35
100	1.4751	3

u_c – Relative combined standard uncertainty
U – Relative expanded uncertainty

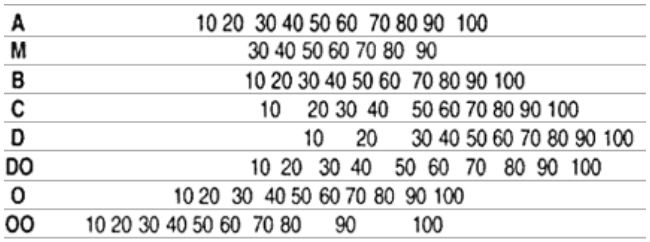

FIGURE 2: QUALITATIVE COMPARISON OF DUROMETER SCALES.

while each scale is internally linear, they are not necessarily linear with each other and that the standard tolerance on one scale does not equate to the standard tolerance on another scale. The drawbacks for this method are numerous, including the inability to measure actual parts and exceptionally large uncertainties (Section 2.2).

FTIR examines the absorbance or reflectance spectrum to identify the chemical make-up then correlates that to a database to determine the material type [15], [16]. This method often requires destructive preparation, requires a library of material spectra, takes a significant amount of time, and can misclassify materials. It is also difficult to ascertain the mechanical properties imparted from processing or manufacture.

2.2 Durometer Uncertainty Quantification

The uncertainty in O-ring durometer is due to four distinct sources: the tolerance, the measurement error, the deformation hardening of polymers, and the use of witness coupons. Witness coupons are never the same shape as an O-ring and experience different material post processing due to cure differences [12].

O-rings procured from a reputable supplier can deviate as much as ±8 durometer from the stated durometer (combined tolerance and measurement error) and can deviate as much as ±16 durometer from the other O-rings in the shipment. This is due to the combined tolerance (non-Gaussian) and measurement error (Gaussian). The industry standard tolerance is ±5 [13], which is attributable to reproducibility issues [17], while the Shore A & D measurement error is generally within ±3 (TABLE 1) for properly calibrated measuring devices [18]. In addition to these issues, some O-ring polymers are very sensitive to temperature fluctuations around room temperature as shown in FIGURE 3 and can vary by as much as 5 durometer.

Misleading hardness measurements due to the deformation of the O-ring is best exemplified by the Shore M results shown in FIGURE 4. Shore M was designed specifically for small specimens such as O-rings, but the measurement can still vary by 40 durometer as the O-ring cross-section decreases. This effect becomes more pronounced for more compliant samples where the measurement can be off by more than 100% of the actual durometer. This makes the Shore M method (as well as other Shore scales) completely unreliable for a significant number of O-rings.

Shore A & D are limited to flat coupons, so a witness coupon is often used. Witness coupon testing, or population sampling, has a low Probability of Detection since the witness

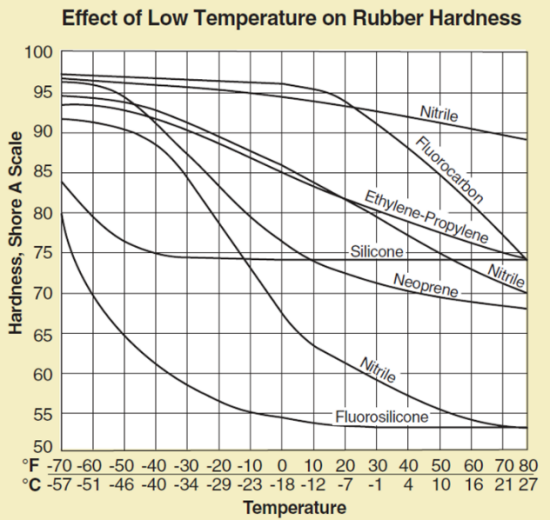

FIGURE 3: TEMPERATURE DEPENDENCE OF POLYMER DUROMETER [13].

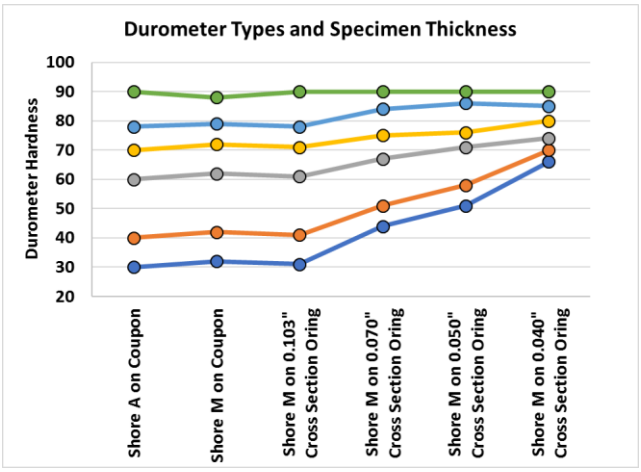

FIGURE 4: INFLUENCE OF SPECIMEN THICKNESS ON DUROMETER MEASUREMENT. EACH LINE REPRESENTS THE NOMINAL DUROMETER. (RECREATED FROM APPLERUBBER.COM)

coupons or selected parts are not necessarily representative of the entire population. In fact, witness coupons are cured differently than O-rings due to shape differences [12]. Some companies perform destructive tests on a few components from a batch and disposition the entire batch based on the results. In a worst-case scenario, this is a false negative rate of nearly 100%.

2.3 Process Compensated Resonance Testing

Resonant Ultrasound Spectroscopy (RUS) is a full-body inspection method popularized by Albert Migliori (Los Alamos National Lab) in the 1980's. The method is predicated on the physical principle that any rigid, elastic body will resonate at specific frequencies that are a function of geometry, mass, material properties, and defects/damage. RUS drives a part to resonate and maps out the resonance spectrum.

Resonance methods were selected for this project due to the intimate relationship between a part's mechanical properties (e.g. stiffness/durometer) and its resonance behavior. In fact, anything that affects the mechanical behavior (at least the static behavior) will influence the resonance spectrum. As such, RUS is often used for material characterization.

The Vibrant approach to RUS, referred to as Process Compensated Resonance Testing (PCRT), applies statistical analyses and machine learning to RUS data in order to identify defects in the presence of acceptable process/population variations. Vibrant also employs a stepped-frequency sine wave excitation for improved frequency resolution and accuracy.

The application of RUS and PCRT for NDT&E is described by several ASTM standards [19] - [21]. PCRT has also been described in several recent publications [22] - [24]. In this paper, we describe an extension of PCRT to characterizing filters as opposed to the resonating bodies themselves.

TABLE 2: LIST OF MATERIAL AND DUROMETER GROUPS.

	Material Groups			Durometer Groups	
	Material	Count		Durometer (±5)	Count
1	BunaN	342	1	65A	97
2	CRBunaN	31	2	70A	577
3	EPDM	148	3	75A	143
4	Florosilicone	32	4	80A	19
5	Polyurethane	31	5	90A	21
6	PTFE	33	6	98.5A	33
7	Silicone	130			
8	Viton	143			

3 MATERIALS AND METHODS

3.1 Materials

The samples examined in this study included eight separate material types and six durometers that were grouped into 11 distinct material-durometer classes. The materials and durometers are presented in TABLE 2. Multiple ages and batches were included in the sample populations to provide process variation but were not considered for analysis purposes. This was done to demonstrate characterization capabilities in the midst of normal process variation.

"Dash-ten" (-10) O-rings (cross-section = 0.070", inner diameter = 0.239", outer diameter = 0.379") were chosen for this study in part due to their wide availability in many materials and durometers. Variations in size and geometry were not included since this study focused on distinguishing nearly identical O-rings and detecting substandard, nonconforming, improperly processed, or counterfeit parts.

The durometer provided by the manufacturer was the "nominal durometer" for the O-rings determined by Shore A measurements on witness coupons with a standard tolerance of ±5. This meant that the true durometer of each O-ring was *UNKNOWN* and that there was a significant likelihood of cross-over between durometer groups separated by 5A (e.g. 65A & 70A or 70A & 75A). The combined tolerance (non-Gaussian) and measurement error (Gaussian) indicates that there may have been cross-over between groups separated by 10A (e.g. 65A & 75A).

3.2 Linear Systems Approach

Soft polymers are viscoelastic in nature, highly attenuative, and difficult to drive to resonance. Given these difficulties for standard ultrasonic inspection in general and resonance inspection in particular, a new approach was needed. For this work we employed the linear system model popularized by Schmerr & Song [25]. The PCRT system used in this study can be characterized as a linear system since it met the homogeneity, additivity, and shift invariance requirements for linear systems. With this approach, we treat the system as a linear elastic system and the soft polymer as a filter placed in the system. Thus, we can extract the acoustic-elastic transfer function for the O-ring.

The received spectral signal ($V_R(\omega)$, where ω is the circular frequency) is influenced by the signal generation process, the cabling, the reception process, and the signature of the part under examination. The received voltage signal therefore contains the transfer functions for the system, $S(\omega)$, and the propagation/filter, $R(\omega)$, in addition to the input voltage function, $V_I(\omega)$. The filter characteristic function can then be extracted by deconvolving (spectral division) the input signal and system function from the received signal (Eq. 1a). A Weiner filter is used to reduce the sensitivity of the deconvolution to signal noise (Eq. 1b).

In practice, it is simpler to calibrate the system than it is to develop a system model. This involves collecting two signals, one with the O-ring (V_{R2}) and another without (V_{R1}). The characteristic function of the O-ring can then be extracted by deconvolving the first signal from the second (Eq. 2a), again using a Weiner filter to reduce noise (Eq. 2b).

$$V_R(\omega) = S(\omega)R(\omega)V_I(\omega) \rightarrow R(\omega) = \frac{V_R(\omega)}{S(\omega)V_I(\omega)} \quad (1a)$$

$$R(\omega) = \frac{V_R(\omega)conj(S(\omega)V_I(\omega))}{|S(\omega)V_I(\omega)|^2+\varepsilon^2 max\{|S(\omega)V_I(\omega)|^2\}} \quad (1b)$$

$$\frac{V_{R2}(\omega)}{V_{R1}(\omega)} = \frac{S(\omega)R(\omega)V_I(\omega)}{S(\omega)V_I(\omega)} \quad (2a)$$

$$R(\omega) = \frac{V_{R2}(\omega)conj(V_{R1}(\omega))}{|V_{R1}(\omega)|^2+\varepsilon^2 max\{|V_{R1}(\omega)|^2\}} \quad (2b)$$

3.3 Experimental Configuration

The experimental configuration used in this study comprised a standard Vibrant PCRT system and custom transducers. The general flow diagram of the system is shown in FIGURE 5. A stepped-frequency sine wave was used to excite resonance in the drive transducer. These displacements were

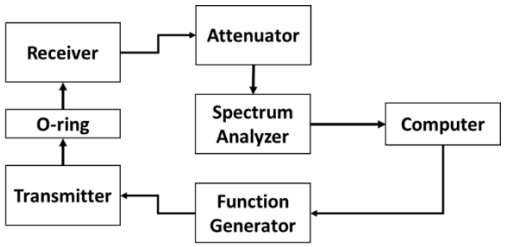

FIGURE 5: BLOCK DIAGRAM OF THE PCRT SYSTEM CONFIGURATION.

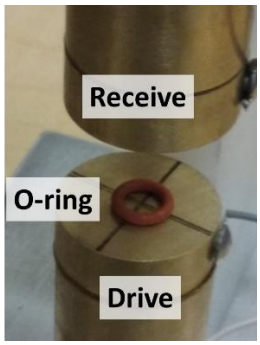

FIGURE 6: ULTRASONIC TRANSDUCER ASSEMBLY WITH O-RING SAMPLE.

dampened by the O-ring as they propagated to the receiver. The received signals were then collected and processed with a spectrum analyzer and the resultant frequency-dependent amplitude recorded. Data was collected via a series of 15 windows centered around the resonance peaks with a total collection range of 15-288 kHz. Each window utilized a boxcar function with widths less than 5 kHz.

Both transmitting and receiving transducers were fabricated with PZT crystals (fc ≈ 124.5 kHz) and large brass masses which acted as resonating bodies. The O-rings were then placed between the transducers with either dry or wet (water) contact as shown in FIGURE 6. Wet contact improved signal amplitude, but did not affect the results.

3.4 Signal Features

Signal features are characteristic aspects of a given signal. The standard signal feature employed by RUS and PCRT is the center frequency of the resonance peak as shown in FIGURE 7.

In this work we extracted the signal features for O-rings by first deconvolving the system function from the received signal then processing the resultant signal. An example feature extraction is signal regression to a known function such as a Lorentzian (FIGURE 7). The parameters of the Lorentzian regression (i.e. center frequency, amplitude, and Full-Width-Half-Max) are then the signal features. Additional signal features include the signal energy (squared integral), the average

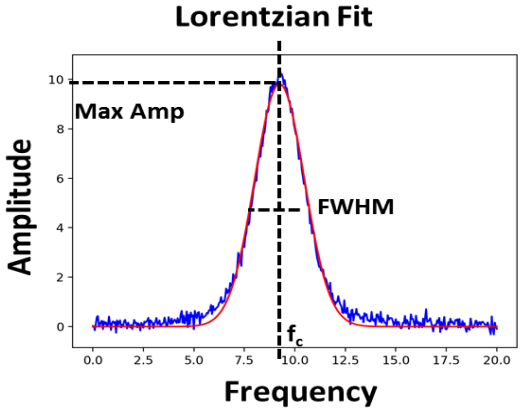

FIGURE 7: EXAMPLE SIGNAL FEATURE EXTRACTION VIA LORENTZIAN FIT.

amplitude, the centroidal frequency for multi-Lorentzian signals, and amplitude variance. In total, 21 features were extracted from each window, which yielded 315 total signal features that were fed into the machine learning algorithm.

3.5 Machine Learning

The machine learning algorithm employed in this work was a Random Forest algorithm [26], [27] as implemented by the SciPy machine learning library [28], [29]. This algorithm was chosen for its multinomial classification and characterizationcapabilities. A Random Forest is a democracy of decision trees that have been grown based on a training set of measured/extracted features and known part characteristics. Each tree was grown based on a subsample of the training set so they were not identical. The general algorithm is shown graphically in FIGURE 8.

Once the forest is trained, it can be used either for multinomial classification or for regression (characterization). In both cases, input is collected from all of the trees in the forest. For multinomial classification forests, unknown parts are sorted into one of N groups based on the majority vote of the trees. This results in an MxN logical array for M parts and N classifications. For characterization forests, the properties of unknown parts are estimated via a regression of the trees (generally an average). This results in an MxL number array for M parts and L properties. Characterization forests can be used to estimate multiple properties at the same time, but generally at the expense of larger forests and/or an increase in the number of required input features.

A supervised learning approach was implemented to grow three different forests of 500 trees each. The first forest was a multinomial classification forest with 11 classifications. The second and third forests were regression forests to estimate durometer and mass respectively. Each of the forests were trained on randomly selected parts that comprised ~50% of the total population. For the multinomial classification, the training set included ~50% of each classification.

It is easy to see that the forest is generally robust since each tree is trained on a different subset of parts, but cross-validation is still necessary. Cross-validation helps to estimate the skill of a machine learning model on unseen data. A standard k-fold cross-validation with 5 folds was employed in this work. This partitions the training set into 5 equal sized subsets, retrains 5 forests on 4/5 sets, and validates on 1/5 sets. The folds do not have overlapping validation parts and thus the sensitivity of the model to each part can be determined in a small number of iterations.

3.6 Analysis

Three analyses are examined in this work: material-durometer classification, durometer estimation, and mass estimation. Although mass/weight can easily be measured using a scale, this analysis was included to demonstrate additional characterization capabilities. All three analyses can be run simultaneously so that the material, durometer, and mass can be ascertained in roughly the same amount of time required to determine the mass with a scale.

After initially training the forests using all 315 extracted features, the contribution of each feature to each of the final forests was calculated. The top 25 contributing features were selected for each forest and the forests were retrained. The features were limited to those whose contribution was $\geq$ 1%. These features represented ~85% of the model information for each forest. Downselecting features decreased scan times while maintaining good results on the training sets. Using all of the contributing features may increase the accuracy of the forests by 1-2%.

Subsequent to retraining the forests on ~50% of the population and 25 signal features, all 890 parts were fed back into the forests. Reanalyzing the training set provided a metric for how well the forest was trained, which could be used as a baseline for the expected performance of the test parts. Analyzing the test parts provided a level of model validation and indicated the performance of the model on future unknown parts.

No tuning of the Random Forests was performed in this work in order to ascertain the baseline capabilities of this approach to characterizing polymer O-rings. There were several parameters that controlled how each individual tree grew and

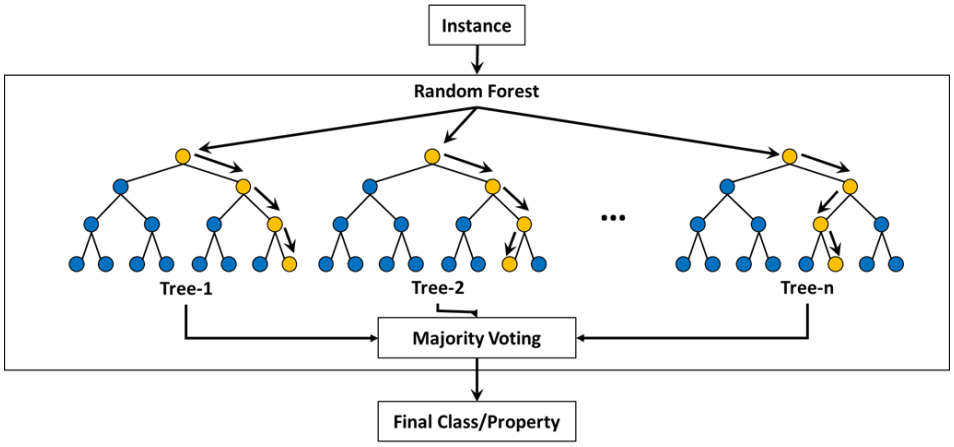

FIGURE 8: SIMPLIFIED FLOW CHART OF A RANDOM FOREST ALGORITHM.

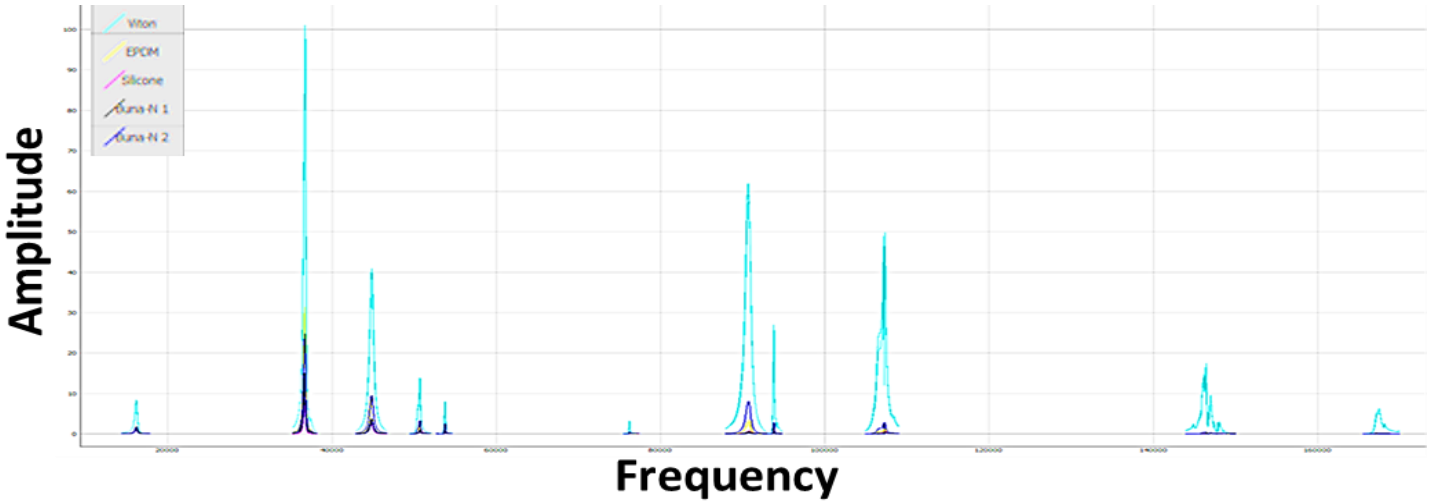

FIGURE 9: TYPICAL COLLECTED SIGNALS FOR SEVERAL MATERIALS.

how different the trees were from each other. Tuning would have helped find the optimal values for those parameters to achieve the sorting goals. With proper tuning, the accuracy of all three Random Forests can be expected to increase by several percent if not more.

4 RESULTS AND DISCUSSION

4.1 Scan Results

Typical results from a resonance sweep of polymer O-rings using the system described above is shown in FIGURE 9. Several materials (indicated by color) were overlaid to show the relative differences. Recall that 21 signal features were extracted for each collection window, 11 of which are shown.

The example spectral plot (FIGURE 10) highlights some drastic differences in the received signal for 4 of the material of material type, there was not a single feature that could correctly sort all of the parts. No single feature contributed more than 10% to any model. FIGURE 10 also exemplifies the level of signal variation within each of the subpopulations due to age and batch variations.

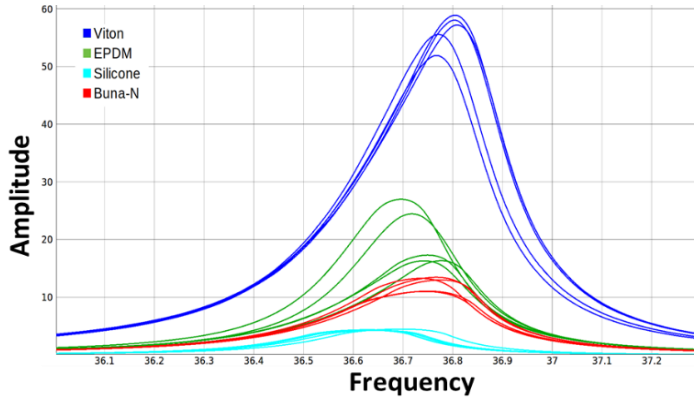

FIGURE 10: EXAMPLE OF A SECTION OF THE SPECTRA FOR O-RINGS. COLORS INDICATE MATERIAL TYPE.

4.2 Multinomial Classification

A multinomial classification sort was created using the Random Forest Classification approach. Note that the forest was trained to the "nominal durometers" provided by the manufacturer. Once the forest was trained, all of the parts were sorted and the results tabulated into a confusion matrix (TABLE 3). The left-hand labels indicate the true classification while the top labels indicate the sorted classification. The classification counts were then normalized to the true part count for each group (far-right column). Each row indicates what fraction of a given group were sorted into which classification and the green diagonal cells indicate what fraction of each group was correctly sorted. The off-diagonal cells indicate mis-sorts.

The overall accuracy of the sort was 92.8%, which includes both training and test parts. 70A Silicone and 80A EPDM exhibited the best performance with 100% accuracy while 70A polyurethane exhibited the worst performance with 81% accuracy. Accuracy of the test parts was slightly lower than the overall accuracy with 84.6%.

There were two likely sources of error for this sort. Inherent uncertainty in the durometer due to the tolerance and measurement error on the part of the OEM meant that there was a significant likelihood of overlap between durometer groups (e.g. 65A & 70A) for the same material. There was also potential overlap of durometer groups separated by 10A. If allowances were made for an uncertainty of ±5 in durometer, then the accuracy of the test parts increased from 84.6% to 90.1%. The second likely source or error for this sort was material similarity between some groups (e.g. CR-BunaN & BunaN).

Live testing was performed using 50 of the training parts and 100 previously untested parts, both of which spanned the 11 material-durometer groups. The test took ~10s per part once the part was loaded. Results from the live testing were 100% and 98% accuracy for the training parts and previously untested parts respectively.

These results (both live and off-line) were quite good for an untuned model. The likelihood of correctly classifying a single

TABLE 3: RESULTS OF O-RING MULTINOMIAL CLASSIFICATION SORTING USING A RANDOM FOREST ALGORITHM. THE HIGHLIGHTED CELLS INDICATED THE FRACTION OF PARTS CORRECTLY SORTED FOR EACH CLASSIFICATION.

		Sorted Classification											**#Samples per Actual Class**
		65A **BunaN**	70A **BunaN**	90A **BunaN**	70A **CRBunaN**	70A **EPDM**	80A **EPDM**	70A **Florosilicone**	70A **Polyurethane**	98.5A (55D) **PTFE**	70A **Silicone**	75A **Viton**	
Actual Classification	65A **BunaN**	**0.89**	0.09	0	0	0	0	0	0.02	0	0	0	**97**
	70A **BunaN**	0.02	**0.91**	0	0.01	0.05	0	0.01	0	0	0	0	**224**
	90A **BunaN**	0	0	**0.95**	0	0	0	0	0	0.05	0	0	**21**
	70A **CRBunaN**	0.10	0.06	0	**0.84**	0	0	0	0	0	0	0	**31**
	70A **EPDM**	0	0.11	0	0	**0.89**	0	0	0	0	0	0	**129**
	80A **EPDM**	0	0	0	0	0	**1.00**	0	0	0	0	0	**19**
	70A **Florosilicone**	0.03	0	0	0	0	0	**0.94**	0.03	0	0	0	**32**
	70A **Polyurethane**	0.19	0	0	0	0	0	0	**0.81**	0	0	0	**31**
	98.5A (55D) **PTFE**	0	0	0.06	0.03	0	0	0	0	**0.88**	0	0.03	**33**
	70A **Silicone**	0	0	0	0	0	0	0	0	0	**1.00**	0	**130**
	75A **Viton**	0	0	0	0	0	0	0	0	0.01	0	**0.99**	**143**
#Samples per Sorted Class		**101**	**229**	**22**	**29**	**125**	**20**	**32**	**28**	**31**	**130**	**143**	**890**

part randomly was ~9.1% while the likelihood of correctly sorting 10 parts randomly is 3.86E-11. This demonstrated the feasibility of using resonance to classify O-rings in production or maintenance environments.

4.3 Durometer Estimation

A durometer estimation analysis was created using the Random Forest Regression approach. Keep in mind that the forest was trained to the "nominal durometers" provided by the manufacturer. Once the forest was trained, all of the parts were analyzed using the regression model and the results summarized in FIGURE 11 and tabulated in TABLE 4.

FIGURE 11 plots the nominal durometer vs. the average estimated durometer for each durometer group. The error bars represent the maximum differences between the nominal and estimated durometer for each group and the dashed lines represent the ±5 tolerance. The vast majority of durometer estimates fell within the tolerance of the nominal durometer.

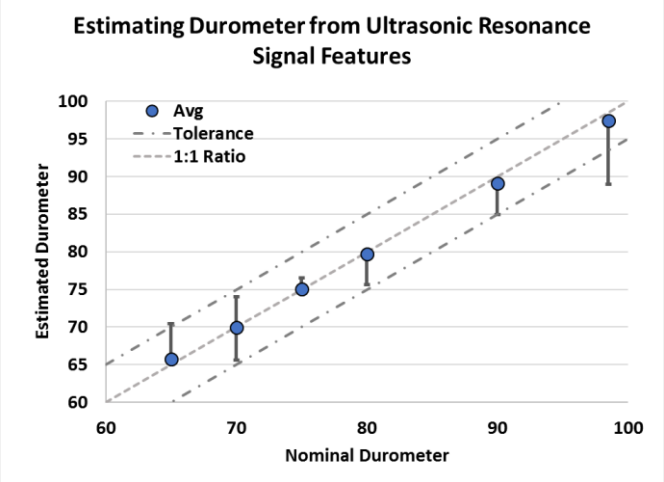

FIGURE 11: DUROMETER ESTIMATES FOR POPULATIONS OF O-RINGS USING ULTRASONIC SIGNAL FEATURES.

TABLE 4 tabulates the results by distinct material-durometer groups. All numbers were normalized to the total population and the relative size of each group is provided for reference. The overall accuracy of the durometer estimation was 99.4% within 5.0 of the nominal durometers (the standard durometer tolerance) and 81.2% within 0.1. Estimation accuracy of the test parts was nearly as good as the overall accuracy with 98.8% falling within 5.0 of the nominal durometers and 84.6% of estimates falling within 0.1. Only 0.6% of total parts (1.2% of test parts) fell outside the ±5.0 tolerance, all of which came from the 98.5A PTFE group. This fallout was likely due to the higher

TABLE 4: DUROMETER ESTIMATION BREAKDOWN BY MATERIAL-DUROMETER GROUPS AS A FRACTION OF THE ENTIRE POPULATION.

Durometer	**Material**	**% of Total Population**	**Estimation Results (%)**		
			Within ±0.1	**Within ±5**	**Outside ±5**
65A	BunaN	10.90	6.29	4.61	0.00
70A	BunaN	25.17	21.24	3.93	0.00
90A	BunaN	2.36	1.35	1.01	0.00
70A	CR-BunaN	3.48	1.80	1.69	0.00
70A	EPDM	14.49	12.13	2.36	0.00
80A	EPDM	2.13	1.69	0.45	0.00
70A	Florosilicone	3.60	3.37	0.22	0.00
70A	Polyurethane	3.48	2.13	1.35	0.00
98.5A (55D)	PTFE	3.71	2.70	0.45	0.56
70A	Silicone	14.61	13.82	0.79	0.00
75A	Viton	16.07	14.72	1.35	0.00

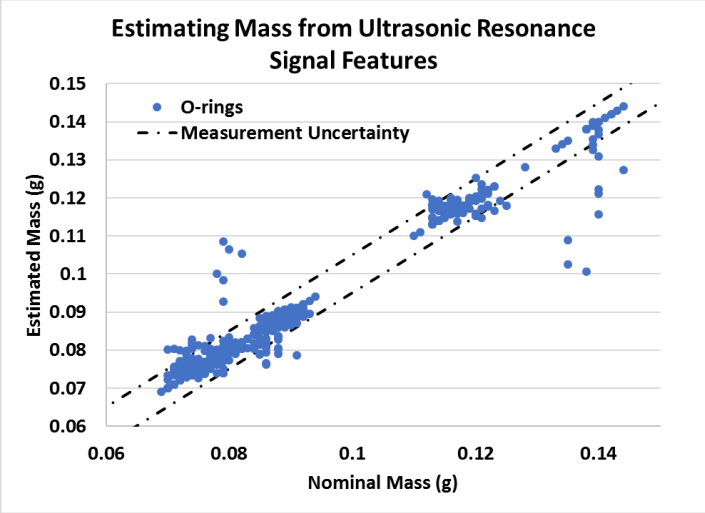

FIGURE 12: MASS ESTIMATES FOR O-RINGS USING ULTRASONIC SIGNAL FEATURES.

relative uncertainty in the durometer measurement near the top of the Shore A scale (100).

Live testing was performed using 50 of the training parts and 100 previously untested parts, both of which spanned the 11 material-durometer groups. The test took ~5 s per part once the part was loaded. Of the 50 training parts, 100% fell within 5.0 A and 98% fell within 0.1A. Testing the previously untested parts resulted in 99% of parts within 5.0A and 94% within 0.1A.

These were remarkable results given the difficulties in measuring durometer in general and the durometer of O-rings in particular. Also noteworthy was that the resonance durometer measurements had a higher resolution than the Shore measurement and were potentially more accurate. Additional study is warranted. The use of Shore A coupons along with a well calibrated Shore A measure would greatly assist in validation.

4.4 Mass Estimation

A mass estimation analysis was created using the Random Forest Regression approach. Once the forest was trained, all of the parts were then fed back through the regression model and the results summarized in FIGURE 12 and tabulated in TABLE 5.

FIGURE 12 plots the measured mass vs. the estimated mass where the dashed lines represent the ±5 mg measurement uncertainty from the scale. This analysis exhibited a little more fallout than the durometer analysis, but still yielded good results for an untuned model.

TABLE 5 breaks the results down by each of the distinct material-durometer groups. All numbers were normalized to the total population and the relative size of each group is provided for reference. The overall accuracy of the mass estimation was 94.0% within 5.0 mg of the nominal mass and 61.1% within 0.5 mg. The estimation accuracy of the test parts was not quite as good with 87.4% falling within 5.0 mg of the nominal mass and 17.8% of estimates falling within 0.5 mg. Approximately 6% of total parts (12.6% of test parts) fell outside the ±5.0 mg

TABLE 5: MASS ESTIMATION BREAKDOWN BY MATERIAL-DUROMETER GROUPS AS A FRACTION OF THE ENTIRE POPULATION.

Durometer	Material	% of Total Population	Estimation Results (%) Within ±0.5 mg	Within ±5 mg	Outside ±5 mg
65A	BunaN	10.90	7.53	3.26	0.11
70A	BunaN	25.17	15.17	8.88	1.12
90A	BunaN	2.36	1.12	0.56	0.67
70A	CR-BunaN	3.48	1.80	1.12	0.56
70A	EPDM	14.49	8.99	4.27	1.24
80A	EPDM	2.13	1.35	0.67	0.11
70A	Florosilicone	3.60	2.36	1.24	0.00
70A	Polyurethane	3.48	2.36	1.12	0.00
98.5A (55D)	PTFE	3.71	2.13	0.45	1.12
70A	Silicone	14.61	9.44	5.17	0.00
75A	Viton	16.07	8.88	6.18	1.01

measurement uncertainty, and came from multiple material/durometer groups. 98.5A PTFE & 90A BunaN had the highest fallout percentage per group with 30.3% and 28.6% respectively, but only accounted for 1.8% of the total fallout. 70A BunaN, 70A EPDM, and 75A Viton each contributed ~1% to the total fallout.

Live testing was performed using 50 of the training parts and 100 previously untested parts, both of which spanned the 11 material-durometer groups. The test took ~5 s per part once the part was loaded. Mass estimates for all 150 parts fell within 5.0 mg of the measured mass.

These are great results given that the mass of a polymer specimen was deduced from a resonance measurement. This demonstrates the potential diverse characterization capabilities of our method. All three of the above analyses can be run simultaneously in roughly the same amount of time it takes to use a scale to determine the mass.

5 Conclusion

Polymer O-rings comprise an entire class of components (including some with safety/mission critical applications) that is currently underserved by NDT&E. Although polymeric O-rings have historically been difficult to characterize via nondestructive means (particularly ultrasonic means), this paper presents a novel approach. The results discussed herein unequivocally demonstrate that ultrasonic resonance methods are sensitive to material differences in polymer O-rings. Both manufactures and consumers of O-rings can utilize this method for process control and material/property verification. There is also the potential to use this method to estimate other desired properties.

This preliminary study used RUS and machine learning to sort O-rings based on material and durometer into 11 distinct classifications with 93% accuracy using a test that took less than 10s per part. In addition to the multinomial sort, this work correctly estimated both the mass (94% fell within 5 mg) and durometer (99% fell within the tolerance of 5) using a test that took less than 5 s.

These results can likely be improved upon by implementing several small changes.

- Tuning the forest growth parameters will likely improve the results by a few per cent.
- Increasing the number of trees in the forest may increase the accuracy, but this increase is subject to the law of diminishing returns. Generally, a forest size of 500 trees is past the point of meaningful gains.
- Using all contributing features instead of the top 25 will increase the information available to the forest, but is not guaranteed to increase accuracy. This will, however, increase the scan time.
- Increasing the number of training parts, especially in underrepresented groups will likely have a significant effect on the accuracy of the models.

Given the standard method for determining durometer of O-rings, the results presented in this paper are limited in scope due to the uncertainty of the durometer. The scope of these results is also limited by holding O-ring sizes constant. Future work should focus on verification and validation of the relationship between resonance signal features and polymer material properties. Using Shore A coupons would greatly assist in that effort. Additional topics for future work include identifying the minimum training set required and detecting polymer degradation and age.

ACKNOWLEDGEMENTS

The authors thank Drs. Ping Yang and Robert Bernstein from Sandia National Laboratories for their input and encouragement.

This work was funded through a Defense Logistics Agency (DLA) Phase II Small Business Technology Transfer (STTR), contract SP4701-17-C-0066.

REFERENCES

[1] AIA, *Counterfeit Parts: Increasing Awareness and Developing Countermeasures*, AIA, Arlington, VA, 2011.

[2] Stern, W., "Warning! Bogus parts have turned up in commercial jets. Where's the FAA?," *BusinessWeek*, June 10, '96 issue, 1996.

[3] Bajak, F., "'Bogus Parts' Plague Airlines: Substandard Components Put Public at Risk," *Associated Press* at *Daily News*, 1996.

[4] Mckenzie, V., "Who's Policing Counterfeit Airplane Parts?," *The Crime Report*, 2017

[5] Baker, B. J., "Identifying the Probability of an Accident Occurring with Suspected Unapproved Parts as a Contributing Factor," *Journal of Aviation/ Aerospace Education & Research*, Vol. 10 (2), 2001.

[6] FAA, *Suspected 'Unapproved Parts' Program Plan*, FAA, Washington, D.C., 1995.

[7] OIG, *AV2017049: Enhancements are Needed to FAA's Oversight of the Suspected Unapproved Parts Program*, DOT OIG, Washington, D.C., 2017.

[8] USA v. Cooper, No. 0:04-CR-60114 (Southern District of Florida), 2004.

[9] USA v. Fifeco, No. 2:06-CV-00512 (District of Utah), 2006.

[10] "Freudenberg Introduces Anti-fraud Markings on Seals," *Rubber & Plastics News*, 2009

[11] Violino, B., "Parker Hannifin Embeds RFID Tags in O-Rings," *RFID Journal*, 2013.

[12] Bernstein, Robert. *Private communications*, 2018

[13] *Parker O-Ring Handbook*, Parker Hannifin Corp., Cleveland, OH, 2018.

[14] *Basic Rubber Testing: Selecting Methods for a Rubber Test Program*, Ed. Dick, J. S., ASTM International, West Conshohocken, PA, 2003.

[15] Everall, N., Chalmers, J., Griffiths, P., *Vibrational Spectroscopy of Polymers: Principles and Practice*, John Wiley & Sons, Hoboken, NJ, 2007.

[16] Siesler, H., "Vibrational Spectroscopy of Polymers," *International Journal of Polymer Analysis and Characterization*, Vol. 16 (8), pp. 519-541, 2011.

[17] ASTM D2240-15e1, "Standard Test Method for Rubber Property-Durometer Hardness," ASTM International, 2015.

[18] Mohamed, M. I., Aggag, G. A., "Uncertainty evaluation of shore hardness testers," *Measurement*, vol. 33, pp. 251-257, 2003.

[19] ASTM E2534-15, *Standard Practice for Process Compensated Resonance Testing Via Swept Sine Input for Metallic and Non-Metallic Parts*, ASTM International, West Conshohocken, PA, 2015.

[20] ASTM E3081-16, *Standard Practice for Outlier Screening Using Process Compensated Resonance Testing via Swept Sine Input for Metallic and Non-Metallic Parts*, ASTM International, West Conshohocken, PA, 2016.

[21] ASTM E3213-19, *Standard Practice for Part-To-Itself Examination Using Process Compensated Resonance Testing Via Swept Sine Input for Metallic and Non-Metallic Parts*, ASTM International, West Conshohocken, PA, 2019.

[22] Livings, R., Mayes, A., Biedermann, E., Heffernan, J., Jauriqui, L., Mazdiyasni, S., "Detection of microtexture regions in titanium turbine engine disks using process compensated resonance testing: A modeling study," *45th Review of Progress in Quantitative Nondestructive Evaluation*, Eds. Bond, L., Holland, S., Laflamme, S., paper 020022, 2019.

[23] Heffernan, J., Biedermann, E., Mayes, A., Livings, R., Jauriqui, L., Mazdiyasni, S., "Validation of process compensated resonance testing (PCRT) sorting modules trained with modeled data," *45th Review of Progress in Quantitative Nondestructive Evaluation*, Eds. Bond, L., Holland, S., Laflamme, S., paper 020020, 2019.

[24] Mayes, A., Heffernan, J., Jauriqui, L., Livings, R., Biedermann, E., Aldrin, J., Goodlet, B., Mazdiyasni, S., "Process Compensated Resonance Testing (PCRT) Inversion for Material Characterization and Digital

Twin Calibration," *45th Review of Progress in Quantitative Nondestructive Evaluation*, Eds. Bond, L., Holland, S., Laflamme, S., paper 020019, 2019.
[25] Schmerr, L., Song, J.-S., *Ultrasonic Nondestructive Evaluation Systems*, Springer US, 2007.
[26] Breiman, L., "Random Forests," *Machine Learning*, Vol. 45 (1), pp. 5-32, 2001.
[27] Dangeti, P., *Statistics for Machine Learning*, Packt Publishing, Birmingham, UK, 2017.
[28] Géron, A., *Hands-On Machine Learning with Scikit-Learn & TensorFlow*, O'Reilly Media, Sebastopol, CA, 2017.
[29] *1.11 Ensemble Methods*, Python-Scikit-Learn, 2018, https://scikit-learn.org/stable/modules/ensemble.html#forest.